Electrolyte Engineering Enables High Stability and Capacity Alloying Anodes for Sodium and Potassium Ion Batteries

Lin Zhou,[ab†] Zhen Cao,[c†] Wandi Wahyudi,[c†] Jiao Zhang,[ab] Jang-Yeon Hwang,[d] Yong Cheng,[a] Limin Wang,[ab] Luigi Cavallo,[c] Thomas Anthopoulos,[c] Yang-Kook Sun,[d] Husam N. Alshareef,[c]* Jun Ming[ab]**

[a] State Key Laboratory of Rare Earth Resource Utilization, Changchun Institute of Applied Chemistry, CAS, Changchun 130022, China.

[b] University of Science and Technology of China, Hefei 230026, China.

[c] Physical Science and Engineering Division (PSE), King Abdullah University of Science and Technology (KAUST), Thuwal, 23955-6900, Saudi Arabia.

[d] Department of Energy Engineering, Hanyang University, Seoul 133-791, Republic of Korea.

*To whom correspondence should be addressed: yksun@hanyang.ac.kr; husam.alshareef@kaust.edu.sa; jun.ming@ciac.ac.cn.

ABSTRACT: Development of sodium and potassium ion batteries with greater energy density is gaining great attention. Although recently proposed alloying anodes (e.g., Sn, Bi) demonstrate much higher capacity than classic carbon anodes, their severe capacity fading hinders their practical applications. The failure mechanism has traditionally been attributed to the large volumetric change and/or their fragile solid electrolyte interphase (SEI). However, herein we present a completely new cogitation and approach based on electrolyte engineering to stabilize alloying anodes. This approach results in unprecedented high capacity (>650 mAh g^{-1}) and stability (>500 cycles) of alloying anodes by simply tuning the electrolyte compositions, without the needy for nano-structural control and/or carbon modification. We confirm that the cation solvation structure, particularly the type and location of the anions in the electrolyte, plays a critical role in alloying anode stabilization. We further present a new anionic and alloying anode reaction model showing that the root cause of the capacity fading in these alloys is dictated by the properties of the anions and not only the volume change or fragile SEI effect. Our model elucidates the failure mechanism in alloying anodes and provides a new guideline for electrolyte design that stabilizes alloying anodes in emerging mobile ion batteries.

TOC

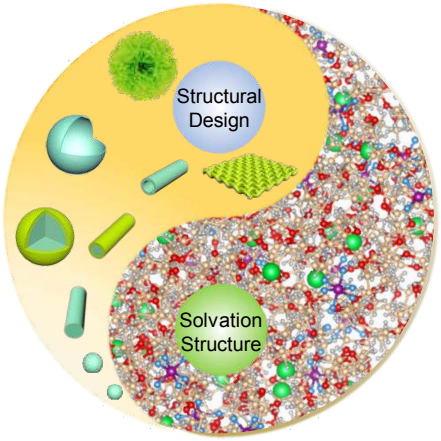

Structural Design ***vs.*** Solvation Structure

Pursuing rechargeable metal-ion batteries with greater energy density is attracting great attention due to increasing demand for energy storage, where alloying anodes can provide very high capacity.[1-7] This is particularly true since sodium and potassium ion battery technologies offer limited capacity and stability using classic carbon-based anodes compared to lithium ions.[8-11] However, alloying anodes are notorious for their severe capacity fading, which has hindered their practical applications. The failure mechanism of alloying anodes has always been ascribed to the large volumetric change (~300%) and/or the fragile solid electrolyte interphase (SEI).[12-15] This interpretation is popular because the pulverization of the alloy-based electrodes can be observed during the reactions. As a result, many strategies have been developed to overcome this issue. These strategies include nano-structural controlling, carbon modification, and improving electrical conductivity. Thus, many nanostructured alloys including particles,[16] fibers/tubes,[5, 17] film/membrane,[18, 19] and hierarchical material[20, 21] are being explored to stabilize alloying anodes. Characteristic, conductive and/or protective materials such as carbon and artificial solid electrolyte interphase (SEI) have been also used to improve alloying anode capacities stabilities.[22-25]

Herein we show that an unprecedented high capacity (>650 mAh g^{-1}) and stability (>500 cycles) can be achieved in alloying anodes by simply tuning the electrolyte composition, without the need for nanostructural control, carbon modification, and/or SEI engineering. We confirm that the cation solvation structure (e.g., Na^+, K^+), particularly the type and location of the anions present in the metal salt and solvents, plays a critical role in affecting the alloying anode performance. In addition, we present a new anionic model showing that the anion corrosion plays at least an equally important role in alloying anode stability as the volume variation and fragile SEI models. Moreover, we present a new reaction model for alloying anode to make the

connections between the electrolyte compositions, SEI chemistry, electrode pulverization, and the stability of alloying anode. Our model provides a different viewpoint to understand alloying anode behaviors. More new insights are presented when we revisit the alloying anode performance in recent literature.[14, 15] We believe that this study not only complements existing knowledge on failure mechanism for alloying anodes but also presents a new principle for electrolyte design to improve alloying anode performance in emerging mobile ion batteries.

RESULTS AND DISCUSSION

Factors affecting alloying anode performance. Alloying anodes with varying nanostructures such as particles[16], fibers[17], tubes[5], films[18], membranes[19], and hierarchical structures[20, 21] have been synthesized to achieve high capacity and stability. Some of these classic strategies to improve alloying anode performance are summarized in **Figure 1**a. However, the capacity, stability and initial Coulombic efficiency of alloying anodes (i.e., <500 mAh g^{-1}, ICE < 60%) still have plenty of room to be improved, even when small areal loading and current densities (less than 1 mg cm^{-2} and 100 mA g^{-1}, respectively) are used (**Table S1**). In contrast, we find that a high capacity and stability can be achieved readily in alloying anodes by electrolyte engineering (i.e., tuning the cation solvation structures as discussed later). For example, using electrolyte engineering strategy, we have been able to achieve areal loading, capacity, and ICE as high as 5 mg cm^{-2}, 650 mAh g^{-1}, and ICE >85%, respectively (**Figure 1**b).

Specifically, we have achieved a high capacity of 700 mA g^{-1} using micro-sized Sn tested at a current density of 500 mA g^{-1} in 1.0 M $NaPF_6$ in dimethoxyethane (DME) electrolyte. A capacity retention as high as 85.3% has been achieved after 200 cycles **(Figure 2**a), where the Coulombic efficiency is higher than 99.8 % (**Figure S1**). The good performance of the alloying anode (e.g., Sn) was also demonstrated under varying active material ratio, areal capacity,

amount of electrolyte used, and rolling process conditions (e.g., the electrode with or without rolling process) (**Figure S2**). In contrast, a severe capacity fading was observed when we changed the metal salt from $NaPF_6$ to $NaCF_3SO_3$ or $NaClO_4$, or when we changed the solvent from DME to the ethylene carbonate/diethyl carbonate (EC/DEC) or propylene carbonate (PC) (**Figure 2**a-d). This result indicates that the electrolyte composition (i.e., solvation structure) is a very important parameter in determining Sn anode performance. This point is further corroborated by results on Bi anode used in sodium and potassium batteries, respectively **(Figure 2**c, e). Firstly, a high capacity of 377 mAh g^{-1} and a high CE of 99.8% can be achieved for micron-sized Bi at a current density of 500 mA g^{-1}, where capacity retention as high as 90.8% can be achieved after 500 cycles (**Figure**. **2**c, **Figure S3**). In addition, a high capacity of 387 mAh g^{-1}, high CE of 99.6%, and good capacity retention of 94.4% after 100 cycles was demonstrated for micron-sized Bi in potassium ion battery (**Figure 2**e, f). However, to obtain these good results, the electrolyte should be 1.0 M MPF_6 (M= Na^+, K^+) in DME. Otherwise, inferior stabilities are observed. This is the case when we use a different electrolyte salt (e.g., $NaCF_3SO_3$ or $NaClO_4$) or solvent (e.g., EC/DEC, or PC) as shown in **Figure 2**c-f. Thus, our preliminarily results show that the electrolyte composition is a very important factor in determining alloying anode stability and performance, and not only volume changes of the anode or SEI effects.

We also considered that the alloying anode capacity fading might result from the electrolyte decomposition on the metal electrode. This is because the interplay of metal electrode and electrolyte has been reported in the literature before.[26-31] We confirm that the capacity fading of the alloying anode might not result from the metal electrode in **Figure S4**. We also demonstrated the superiority of the electrolyte 1.0 M MPF_6 in DME. This is confirmed by the

metal plating/stripping in the asymmetric (i.e., Cu | Na or Cu | K) and symmetric cells (i.e., Na | Na or K | K) (**Figure S5**a-b), which are being widely used in metal batteries (e.g., Li, Na, K batteries).[32-36] We find that the $NaPF_6$ demonstrates higher reversibility and CE compared to other sodium salts such as $NaCF_3SO_3$ and $NaClO_4$, where the DME solvent is always superior to EC/DEC and PC solvent (**Figure S5**c-g). Thus, the capacity fading might result from the difference in electrolyte compositions (i.e., the cation solvation structure, the type of the anions in the electrolyte).

Role of SEI and solvation structure. The role of SEI and electrolyte composition (i.e., solvation structure) in determining alloying anode performance (e.g., Sn, Bi) was investigated in sodium-ion batteries (**Figure 3**a). Firstly, we used the alloying anode to assemble a half cell using the electrolyte 1.0 M $NaPF_6$ in DME for forming an SEI after the 1st cycle (i.e., alloy@SEI in **Figure 3**a). Then, we dis-assembled the battery and used the alloy@SEI anode to assemble new batteries using different electrolytes (e.g., incompatible electrolytes). We find that the alloy@SEI anode demonstrates a fast capacity fading, which is similar to that of fresh alloying anode tested in an identical electrolyte (**Figure 3**b-c). These results show that the formed SEI cannot stabilize the alloying anode if the electrolyte composition is incompatible with the anode. In contrast, we also obtained an alloy@SEI anode by cycling a cell in incompatible electrolyte first and then used the alloy@SEI anode in a compatible electrolyte (i.e., 1.0 M $NaPF_6$ in DME) (**Figure 3**d). We find that the alloy@SEI anode can cycle well in the compatible electrolyte (**Figure 3**e-f). These results demonstrate that the alloy@SEI anodes are stable in compatible electrolytes (e.g., $NaPF_6$) even if the alloy structure was initially destroyed by cycling (for one cycle) in the incompatible electrolyte. In fact, the cycling performance is as good as that of the freshly-prepared alloying anode. Herein, we also considered the possible dissolution and/or

cracking of SEI component that might occur during experiments. This is because the dissolved SEI component can change the solvation structure and possibly affect the electrode performance. Finally, we find that the dissolution and cracking of the SEI component are very limited (**Figure S6**). Thus, these results confirm that the effect of the formed SEI in maintaining anode stability is limited for these alloying anodes, while the electrolyte composition (i.e., solvation structure) is the dominant effect in determining alloying anode performance.

Performance of cycled anodes in different electrolytes. The morphological changes of cycled Sn anodes were examined in different electrolytes (**Figure S7**). We find that, when tested in 1.0 M $NaPF_6$ in DME electrolyte, the micron-sized Sn anode can be pulverized into nanoparticles gradually until it forms a porous and branched structure (**Figure S7**a-c, **Figure S8**). Interestingly, the separator surface remained clean. In contrast, a glossy polymeric gel-like layer that fully covers the pulverized Sn particles was observed in the case of 1.0 M $NaCF_3SO_3$ in DME electrolyte (**Figure S7**d-f),[37, 38] with black impurities covering the separator. The worst performance was observed in 1.0 M $NaClO_4$ in DME electrolyte, where a gel-like layer formed which is too thick to observe the Sn particles, with more black impurities on the separator (**Figure S7**g-i). The black impurities might result from side-reactions, which may be the main reason for capacity fading because we can observe electrode pulverization in all the cases.

These comparative results indicate that the reason for the varying anode stability performance may be related to the different anions present in the electrolyte since the same DME solvent was used for batteries tested in **Figure S7**a-i. One possibility is that some side reactions have occurred between the electrolyte and electrode catalyzed by the corrosion capabilities of the anions. This is a reasonable hypothesis because such phenomena are common in material science; for example, the corrosion of steel in solution is caused by anions.[39, 40] In addition to the

effect of the anions, we further examined the solvent effect when the alloying anode was cycled in 1.0 M $NaPF_6$ in PC electrolyte. We find that the Sn anode is pulverized and black side-products were also formed on the separator (**Figure S7**j-l). This result demonstrates that the solvent can also affect the alloying anode performance, even though the same $NaPF_6$ salt was used in the two solvents (DME and PC). Briefly, we can conclude from the experiments above that the corrosion capability of anions in the electrolyte should decrease in the sequence of ClO_4^- > $CF_3SO_3^-$ > PF_6^-, while the DME is a better solvent for preventing corrosion compared to PC or EC/DEC. This because DME has a stronger interaction with the Na^+ ions, which keeps the anions far from the electrode surface, as discussed later. A similar phenomenon was confirmed by studying the morphological evolution of Bi alloys cycled in various electrolytes (**Figure S9**). We find that the surface of the Bi alloy cycled in 1.0 M $NaPF_6$ in DME electrolyte is smooth without gel-like layer, while a fully covered by-product is observed on the cycled Bi alloy when PC or EC/DEC solvents (instead of DME) were used. Besides the electrode evolution, we further find that the CE and capacity exhibit the same trend. In other words, degradation of the Bi alloy anode is smallest for PF_6^- and largest for $CF_3SO_3^-$ and ClO_4^-; similarly, the Bi alloy anode is most stable in DME compared to EC/DEC and PC solvents. These results demonstrate the better capability of PF_6^- anions, and DME to stabilize Sn and Bi alloying anodes (**Figure 2**, **Figure S7-S10**). Besides, the differences in the electrode can be further observed and analyzed by electrochemical impedance spectroscopy (EIS) and X-ray photoelectron spectroscopy (XPS).[41-45] Our results show that the formed SEI is dependent on the compositions of the electrolyte. Essentially, the different chemical reactions of the cation-solvent-anion that take place on the alloying anode interface give rise to different components and properties of SEI (**Figure S11-S12**).

Role of solvation structure. With the role of anions and solvents demonstrated, we discuss the role of the solvation structure. A redshift of the P-F vibration in the PF_6^- anion from 768 cm^{-1} to 740 cm^{-1} was observed in the Raman spectrum,[45] demonstrating the solvation process, where solid $Na^+PF_6^-$ salt is dissolved into solvated PF_6^- ions in the electrolyte (**Figure 4**a). The PF_6^- anions have a high degree of mobility in EC/DEC and PC compared to DME, as confirmed by the higher wavenumber in DME (at 743 cm^{-1}) compared to 740 cm^{-1} in EC/DEC and PC. This is reasonable because the EC/DEC and PC have a higher capability to dis-associate $Na^+PF_6^-$ because of the high dielectric constant (i.e., ε_{EC}=89.78; ε_{PC}=64.92; ε_{DME}=7.2).[46, 47] In other words, the average distance between Na^+ and PF_6^- in DME solvent (i.e., $Na^+[DME]_{9.61}[PF_6^-]$) is shorter than that in EC/DEC (i.e., $Na^+[EC]_{7.76}[DEC]_{4.13}[PF_6^-]$) and PC solvent (i.e., $Na^+[PC]_{11.75}[PF_6^-]$) due to the low dielectric constant and amount of DME solvent when 1.0 M $NaPF_6$ salt is used (**Figure S13**). However, the Na^+ and PF_6^- is easier to form than the Na^+-PF_6^- contact ion pair[48] in EC/DEC and PC solvent, as confirmed by the FTIR results (**Figure S14**). The PF_6^- has more opportunities to contact with the Na^+ in the first solvation structure when the EC/DEC or PC solvent is used. This is because the steric hindrance existing in the carbonate-based electrolyte (i.e., $Na^+[EC]_{4\text{-}6}$, $Na^+[DEC]_4$ or $Na^+[PC]_{4\text{-}6}$ *via* monodentate chelation) is much less than that in DME-based electrolyte (i.e., $Na^+[DME]_2$ *via* bidentate chelation). In this way, DME can separate the Na^+ and PF_6^- effectively not only in the bulk electrolyte but also on the electrode interface, as discussed later.

Besides, we find that the proportion of the coordinated DME (i.e., Raman peak at 856 cm^{-1}) is the highest in 1.0 M $NaPF_6$ in DME electrolyte (**Figure 4**b).[49] This is because the PF_6^- has the weaker coordination capability with the cation compared to $CF_3SO_3^-$ and ClO_4^-, thereby facilitating good coordination between DME and the cations. In contrast, the $CF_3SO_3^-$ and ClO_4^-

anions can coordinate with the cation competitively and exclude DME out of the solvation structure, thereby giving rise to more free DME. These observations are consistent with the ^{1}H-NMR analysis, in which the shift of CH_3/CH_2 peaks in DME is the most obvious when $NaPF_6$ was used instead of $NaClO_4$ and $NaCF_3SO_3$ (**Figure 4**c). The information on the solvation structure present in different solvents can be obtained from the ^{19}F-NMR of PF_6^- anions (**Figure 4**d). The appearance of the ^{19}F-NMR peak at a low magnetic field (i.e., high extranuclear electron cloud density) in the solvents DME, PC, and EC demonstrates that the cation has good coordination with these solvents. In contrast, the coordination between the branched/linear DEC and the cations is not so condensed, leading to the peak shift towards the higher magnetic field. Thus, we can see a medium ^{19}F- NMR peak shift in the mixed EC/DEC solvent.

Based on these results, the proposed coordination structures are illustrated in **Figure 4**e. Note that this is an average coordination structure for the Na^+ and solvent. We believe that one Na^+ can coordinate with two DME molecules, while one Na^+ can coordinate with four solvent molecules in the case of EC, PC, or DEC, but the DEC-based solvation structure is loose due to the branched structure. These results demonstrate that the Na^+ solvation structure in 1.0 M $NaPF_6$ in DME electrolyte is stable and not so condensed. This means that PF_6^- anions have adequate freedom of movement, while the PF_6^- is not easy to contact with the Na^+ to form the Na^+-PF_6^- contact ion pair due to the bidentate chelation of Na^+-DME. Therefore, the PF_6^- can be always kept a distance from Na^+ even the distance of Na^+ and PF_6^- is short. In contrast, the PF_6^- is relatively easy to contact with Na^+ due to the lower steric hindrance resulting from the monodentate chelation of Na^+-EC or Na^+-PC, even though the distance of Na^+ and PF_6^- might be somewhat large (**Figure 4**e). These viewpoints are consistent with the analysis done by FTIR and ^{19}F- NMR (**Figure S13-S14**, **Figure 4**d). In this way, the PF_6^- demonstrates different

opportunities to contact with the alloying anode interface during the Na^+ desolvation process, and then affect the electrode performance, as discussed later. Thus, we observe that the alloying anode capacity is highest in DME and is lowest in EC/DEC and PC. Besides, a fast capacity decay can be observed when either $CF_3SO_3^-$ or ClO_4^- anions was used. This occurs because the $CF_3SO_3^-$ or ClO_4^- anions can occupy the DME position in the solvation structure, meaning they can affect the alloying anode stability more easily during the de-solvation process. Thus, we believe that the site of anions in the solvation structure plays a key role in determining the Sn and Bi anode performance and stability.

Simulation and interfacial model. Our viewpoint about the solvation structure has also been studied and confirmed by molecular simulations. We show the radial distribution function (RDF) of Na^+ cations to the oxygen in different solvents (e.g., DME, PC, DEC) in **Figure 5**a. The results indicate that DME has the highest occurrence around Na^+ compared to PC and DEC. This is consistent with our coordination model shown in **Figure 4**e, in which we believe that DME has more interaction with the Na^+ ions. In addition, the steric effect of anions (e.g., PF_6^-, $CF_3SO_3^-$ and ClO_4^-) was considered through the buried volume (%VBur) calculations (**Figure 5**b-e), which represents the space occupied by anions immediately coordinated to the central Na^+.[50] We find that a medium %VBur of 26.8% for PF_6^- is observed which corresponds to a medium degree of mobility in the electrolyte. In contrast, the ClO_4^- has a smaller %VBur of 24%, enabling its higher degree of mobility in the electrolyte. Although the $CF_3SO_3^-$ anion occupies a high volume (i.e., %VBur of 28%), the strong interaction between Na^+ and the $CF_3SO_3^-$ anion can compensate for the steric effect and still induce a high appearance frequency around the Na^+. These results are consistent with the Raman and NMR observations.

Particularly, this point was further supported by simulation of the interfacial behaviors on the alloying anode surface when different metal salts ($NaPF_6$, $NaCF_3SO_3$, and $NaClO_4$) were used in DME. We find that the frequency of ClO_4^- and $CF_3SO_3^-$ appearance on the alloying anode surface is much higher than that of PF_6^- (**Figure 5**f-h). This result explains their inferior performance because $CF_3SO_3^-$ and ClO_4^- would be closer to the cations on the anode surface due to their strong coordination capability and a high degree of mobility. In addition to the snapshot, the statics analysis also corroborates this viewpoint. We find that the frequency of anions appearing near the alloying anode is in the sequence of $ClO_4^- > CF_3SO_3^- > PF_6^-$ when the DME solvent is used (**Figure S15**). Thus, the simulations are consistent with our hypothesis, in which the properties of anions play a critical role in determining alloying anode performance.

Finally, we present a solvation structure and an anionic interfacial model to interpret the observed alloying anode behaviors. We use the generic formula $M^+[solvent]_x[anions]$ ($M = Na^+$, K^+) to represent the electrolyte. Our results indicate that the distance between the anions and cations in a solvation structure is smaller for ClO_4^- and $CF_3SO_3^-$ than PF_6^- in DME (**Figure 6**a-c). As a result, PF_6^- is kept farther from the alloying anode surface (green slabs in **Figure 6**) compared to ClO_4^- and $CF_3SO_3^-$ during the de-solvation process. Thus, good stability is obtained in 1.0 M $NaPF_6$ in the DME electrolyte. The molecular interaction can also be described using our model when the EC, EC/DEC or PC solvents are used (**Figure 6**d-f). We propose that the mobility of PF_6^- in these solvents is higher than that in DME, particularly in the interfacial region during the de-solvation process, which leads to a high frequency of PF_6^- occurrence on the alloying surface. This is reasonable because these kinds of solvents cannot form a five-ring complex like DME, meaning PF_6^- cannot be kept far enough from the anode surface. As a result, alloying corrosion and a severe capacity fading are observed. This analysis shows that the type

and position of anions at the alloying anode surface can be controlled by changing the metal salts as well as the solvents. Therefore, we can tune the alloying anode performance by simply changing the composition of the electrolyte. The anions can move close to the alloying anode surface if the anion has a strong coordination capability with the cation (e.g., $CF_3SO_3^-$) and/or high mobility (e.g., ClO_4^-). Similarly, the anions can move close to the alloying anode surface if the solvent has an insufficient coordination capability to exclude the anion (e.g., EC/DEC, PC). Thus, our anionic interfacial model can interpret all the observed alloying anode performance based on the metal salt or solvent that makes up the electrolyte. The rationality of our interfacial model was further demonstrated by changing the type of solvent in the electrolyte. The other kind of ether-based electrolyte (e.g, 1.0 M $NaPF_6$ in diethylene glycol dimethyl ether (DEGDME), and tetraethylene glycol dimethyl ether (TEGDME)) and the effect of different solvent (e.g., DOL, EC, PC,) with different dielectric constant[51-53] were also studied (**Figure S16**). The observed alloying anode perofmrance in **Figure S16** are consistent with our interfacial model (**Figure 6**g-i). Based on this model, we can further conclude that the electrolyte decomposition is a solvent-derived process, which can be affected directly by the anionic characteristics (e.g., properties, positions) and the type of solvent.

Alloy reaction model. Additional insight can be gained into our model when we consider the classic literature on electrolyte and SEI chemistry.[54-61] We present a new reaction process model for alloying anode to understand the relations between the electrolyte properties, SEI chemistry, electrode pulverization, and the stability of alloying anode. We can classify two types of sites on the surface of the pristine alloying anode: i) fresh site, which has the same properties as the bulk phase. The fresh site will be stable when the electrolyte is compatible with the alloying anode (e.g., 1.0 M $NaPF_6$ in DME). As such, there are no side-reactions (i.e., electrolyte decomposition)

that occur at fresh sites, which means there is no SEI formation. In contrast, the fresh site is not stable when the electrolyte is incompatible with the alloying anode (e.g., 1.0 M $NaPF_6$ in $NaClO_4$). In the latter case, e side-reactions (i.e., electrolyte decomposition) can occur on this fresh site, and an SEI can be formed.; ii) active site, which is a site on which the electrolyte can be decomposed due to high reactivity, thus an SEI is formed on the anode surface. Using this classification, the SEI chemistry and alloying anode performance can be related as discussed below.

In the compatible electrolyte, the electrolyte decomposition can occur only on the active sites to form the SEI during the 1st cycle; the fresh site remains stable, and more fresh sites could be formed upon alloying anode pulverization during discharge. In such case, the alloying anode can be stabilized after the 2nd cycle for two reasons: i) the active site becomes stable because the SEI can cover the active site (i.e., active site@SEI) and reaction activities were reduced on the surface, particularly because the electrolyte is anode-compatible; ii) the fresh site remains stable, and no electrolyte decomposition takes place at this site because of the inherent electrolyte compatibility (**Figure 7**a). In contrast, in the case of incompatible electrolytes, the electrolyte decomposition could occur on both the active and fresh sites, giving rise to SEI-coated active site (i.e., active site@SEI) and SEI-coated fresh site (i.e., fresh site@SEI), and newly-formed fresh site due to the alloying anode pulverization. As a result, a low CE (i.e., large irreversibility) is observed in the 1st cycle. In the 2nd cycle, the electrolyte decomposition can occur continually at least on the newly formed fresh site; meanwhile, the electrolyte decomposition can also occur on the active site@SEI and fresh site@SEI due to incompatibility of electrolyte with the alloying anode (**Figure 7**b). As a result, the electrolyte decomposition and severe capacity fading can always be observed upon cycling, as shown in **Figure 2**.

Based on this analysis, several conclusions can be made: i) the electrolyte is the most critical factor in stabilizing the alloying anode; ii) the alloying anode pulverization is not the main cause of capacity fading. In other words, the pulverization is a consequence of the (dis-)charge process under which the exposed fresh site can be stabilized in anode-compatible electrolytes; iii) the formed SEI can reduce the electrode activities and mitigate the electrolyte decomposition, but this positive effect does not take place in anode-incompatible electrolytes; iv) finally, the interplay of metal electrode and electrolyte (e.g., wettability, side-reactions) need to be considered, while the characteristics of alloying anode (e.g., porous integrity) can affect the electrolyte compatibility. In brief, the stability of cation-solvent-anion needs to be considered on the alloying anode and metal electrode both, because it determines the compatibility of electrolyte directly (**Figure S17**). We hope these relations are helpful for designing more versatile electrolyte compatible with the alloying anode and/or other kinds of anode for wider applications.

In summary, we present a new insight into the factors affecting alloying anode performance in metal ion (Na^+, K^+) batteries. We demonstrate that the solvation structure, particularly the type and location of the anions, can be tuned by the metal salt and solvent, and can consequently control the alloying anode performance. Unprecedented high performance is achieved in alloying anodes (e.g., Sn, Bi) without the needy of nanostructural design or carbon modification for the micron-sized alloying anodes. In addition, we introduce a new anionic interfacial model and alloying anode reaction model to interpret the alloying anode morphological and electrochemical performances observed in different electrolytes. Our model presents a new underlying mechanism for the morphological and electrochemical performance of alloying anodes, which complements the well-known volumetric change and/or fragile SEI effects. Our interfacial model

can be used to design electrolyte compositions that preserve the structural stability and improve the electrochemical performance of alloying anodes in mobile ion batteries.

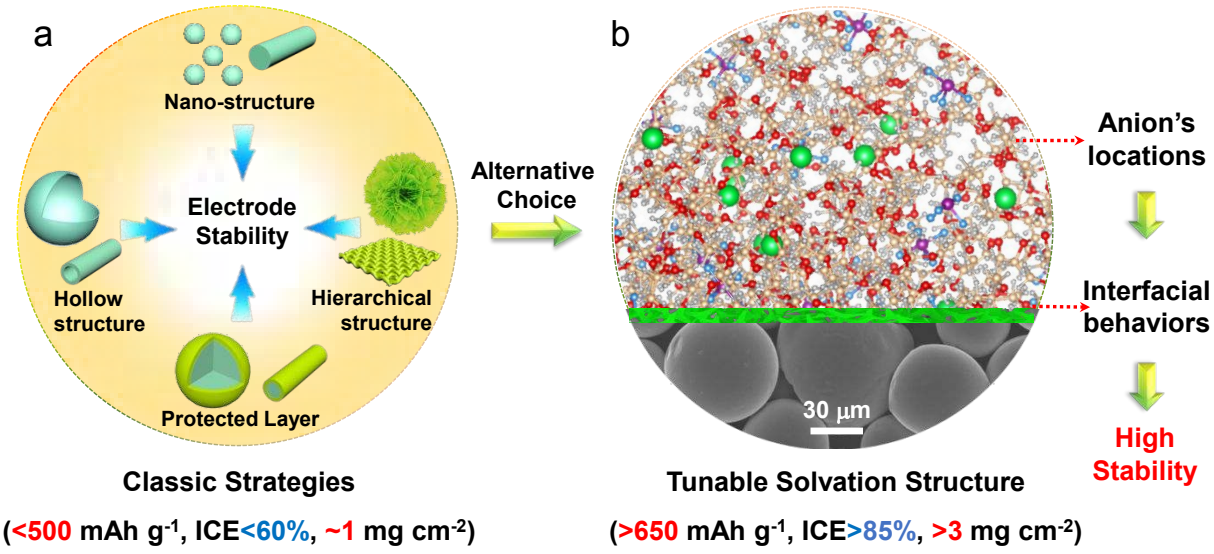

Figure 1. Schematic illustration of strategies used for stabilizing the alloying anodes in mobile ion batteries. (a) Nano-structural control and (b) Tunable solvation structure.

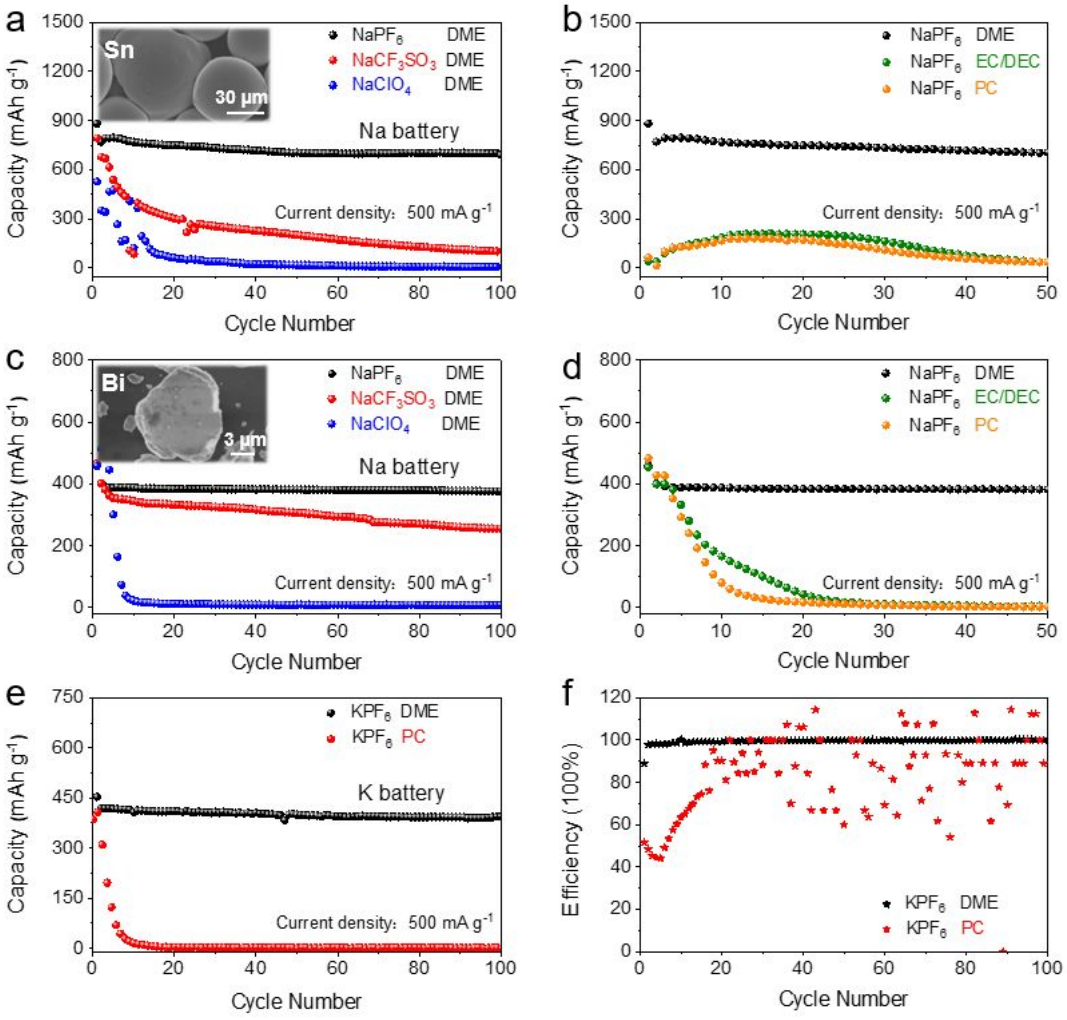

Figure 2. Comparative performance of alloying anodes in different electrolytes. Cycling performance of (a, b) Sn and (c, d) Bi anode in (a, c) 1.0 M $NaPF_6$, $NaCF_3SO_3$ or $NaClO_4$ in DME, and in (b, d) 1.0 M $NaPF_6$ in DME, EC/DEC, or PC, respectively. Insets in (a) and (c) are the SEM images of the micro-sized Sn and Bi particles, respectively. (e, f) Cycling performance and Coulombic efficiency of Bi anode in 1.0 M KPF_6, in DME, or PC, respectively.

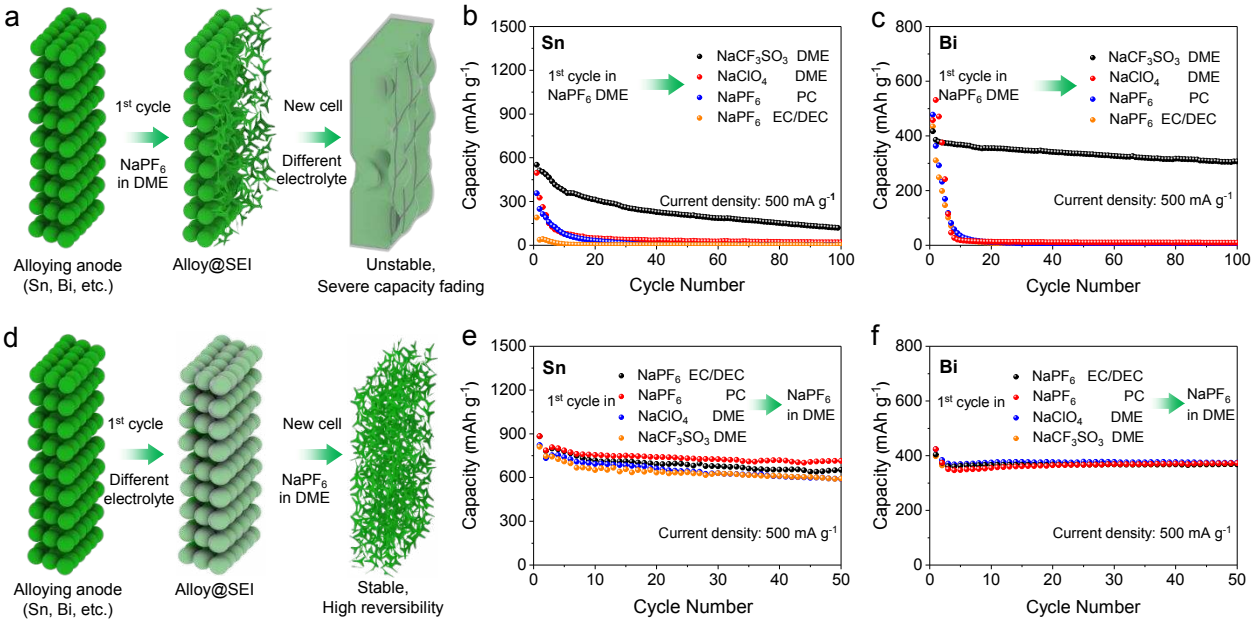

Figure 3. Role of SEI in alloying anode stability. (a) Alloying anodes (Sn or Bi) were cycled in 1.0 M $NaPF_6$ in DME first to form the SEI layer (alloy@SEI electrode). Then we assembled the alloy@SEI electrode in a new battery using a different electrolyte. Cycling performance of the (b) Sn@SEI and (c) Bi@SEI electrodes in different electrolytes. (d) Alloy anode was cycled in different electrolytes first to form the SEI layer, and then we assemble the alloy@SEI electrode in a new battery using 1.0 M $NaPF_6$ in DME electrolyte. Cycling performance of the (e) Sn@SEI and (f) Bi@SEI in the 1.0 M $NaPF_6$ in DME electrolyte.

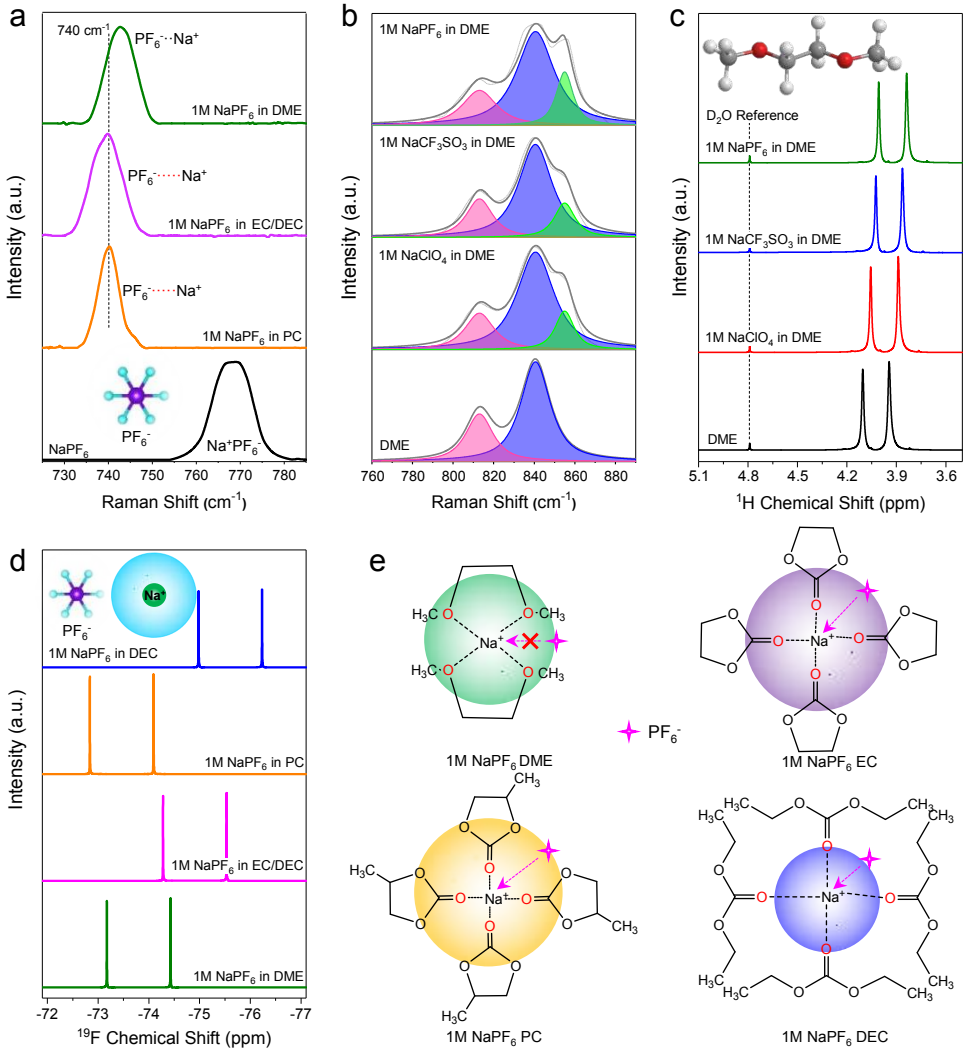

Figure 4. Solvation structure of the cations and solvents. (a) Raman spectra of PF_6^- anions in different kinds of solvents. (b) Raman spectra of CH_2 rocking/C-O stretching vibrations and (c) ^1H NMR spectra of different types of sodium salt in DME a. (d) ^{19}F-NMR spectra of PF_6^- anions in different kinds of solvents. (e) Proposed coordination structure of Na^+-solvents pairs, in which the opportunities of PF_6^- to contact the Na^+ was presented.

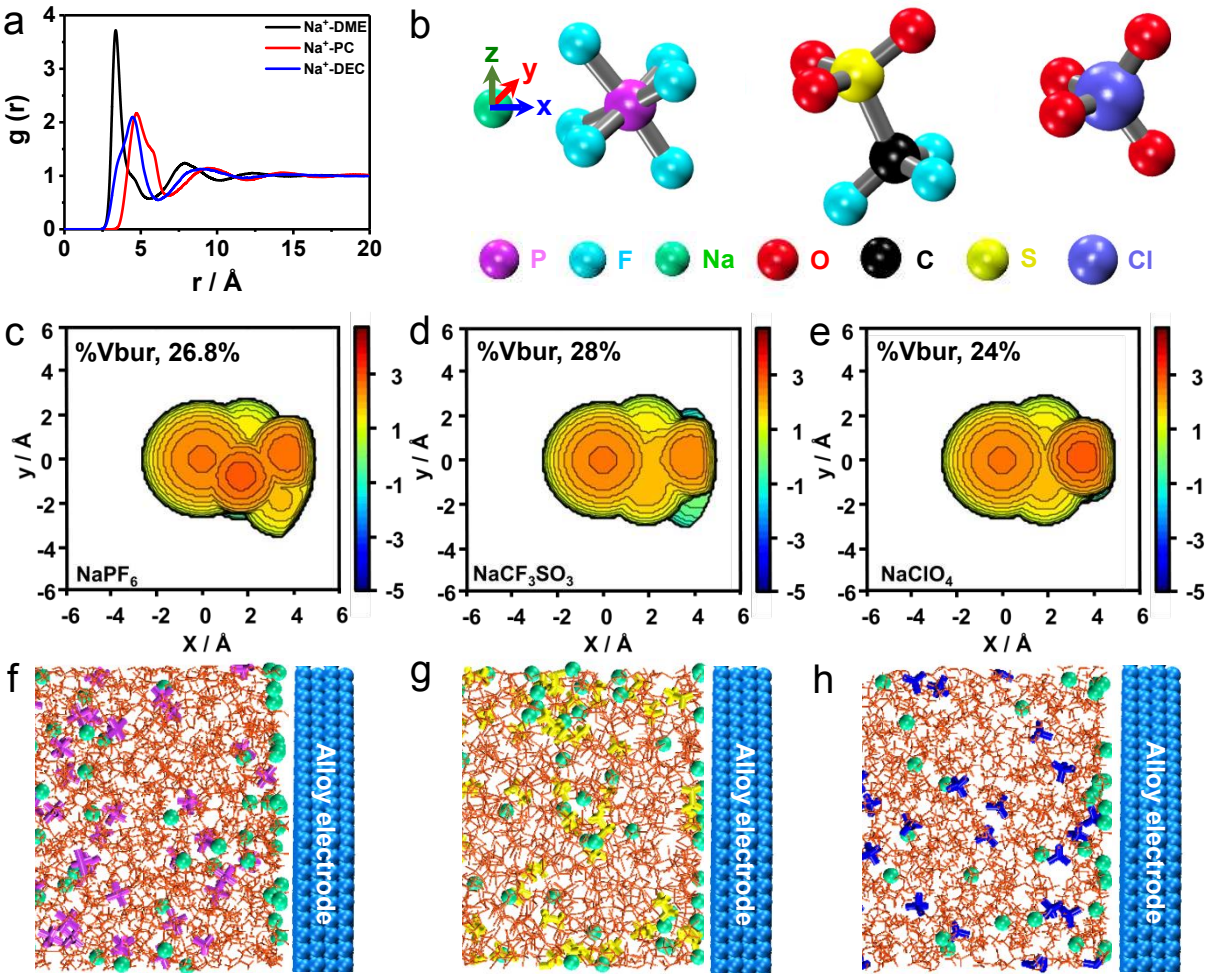

Figure 5. Simulation and interfacial behavior analysis. (a) Radial distribution function (RDF) of Na^+ to oxygen in DME, PC, and DEC, respectively. (b) Illustration of the interaction between the anion and cation. Buried volume (%VBur) calculations for different anions (c) PF_6^-, (d) $CF_3SO_3^-$, and (e) ClO_4^- with the Na^+. Interfacial behavior of molecules on the alloy anode surface in (f) 1.0 M $NaPF_6$ in DME, (g) 1.0 M $NaCF_3SO_3$ in DME, and (h) 1.0 M $NaClO_4$ in DME.

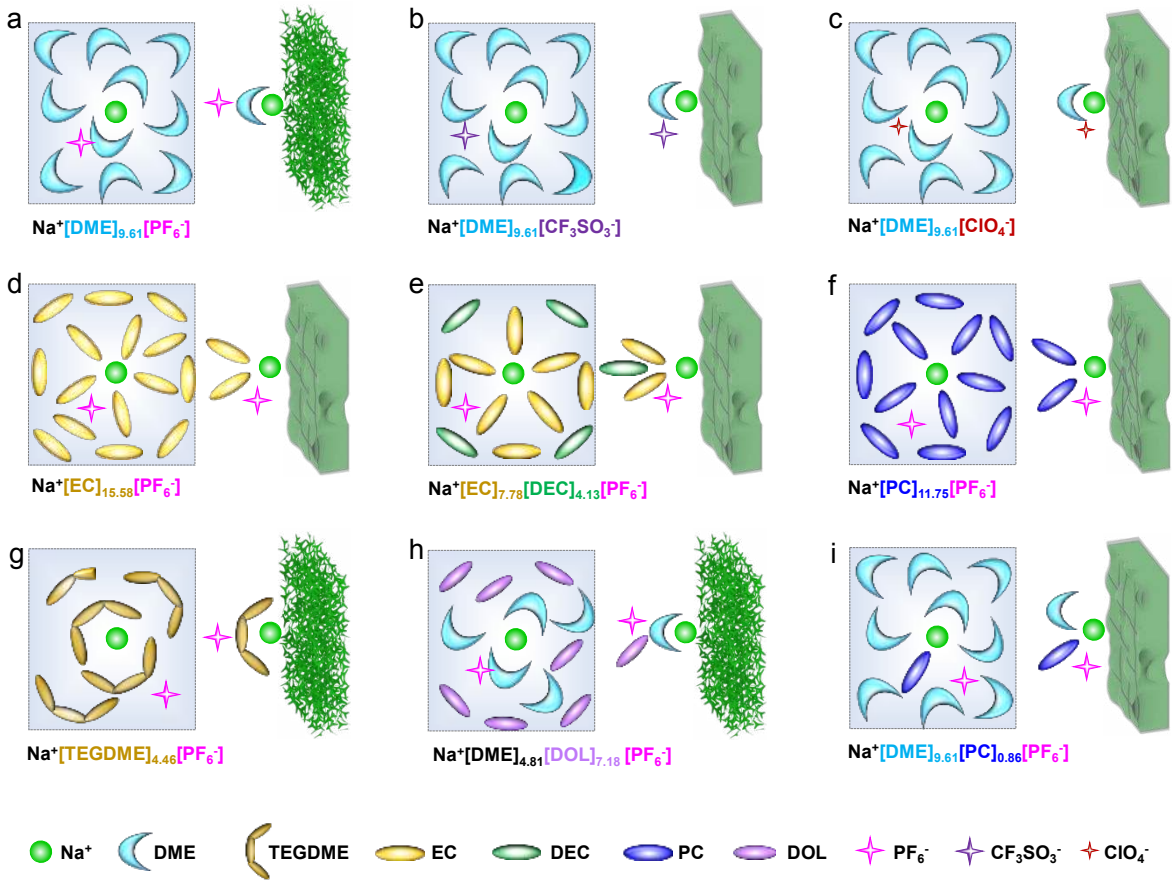

Figure 6. Anionic interfacial model from the bulk electrolyte to the alloy interface. The mode in DME-based electrolyte using different metal salt of (a) $NaPF_6$, (b) $NaCF_3SO_3$, and (c) $NaClO_4$, respectively. The model of $NaPF_6$-based electrolyte using different solvent of (d) EC, (e) EC/DEC, (f) PC, (g) DOL/DME, (h) TEGDME or DEGDME, and (i) PC/DME or EC/DME.

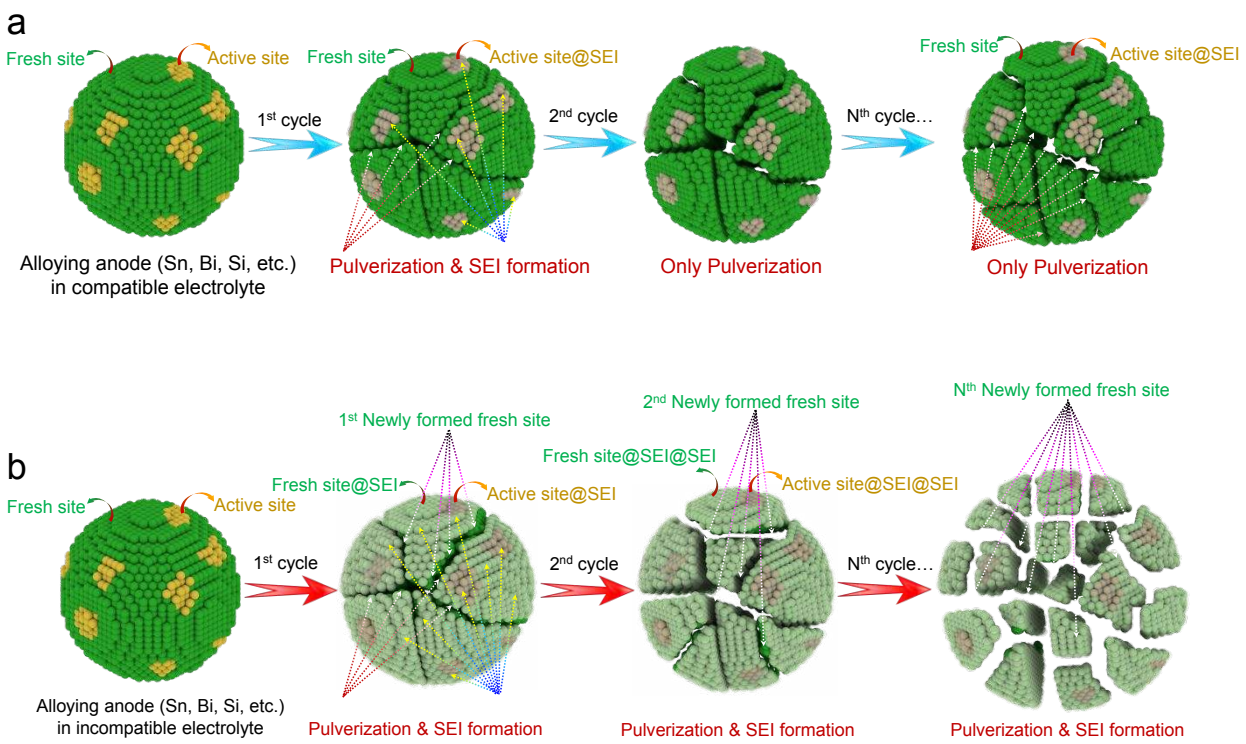

Figure 7. Alloying anode reaction model. Comparative alloying anode behaviors in the (a) compatible and (b) incompatible electrolyte upon cycling. After the 1st cycle, the SEI coated active site (i.e., active site@SEI), original fresh site, the newly-formed fresh site (i.e., caused by electrode pulverization) are all stable upon cycling in compatible electrolytes, thus a good performance can be observed. In contrast, the active site@SEI, original fresh site, the newly-formed fresh site are not stable in incompatible electrolytes, thus a severe capacity fading can be observed.

ASSOCIATED CONTENT

Supporting Information. Experimental and simulation section. **Figures S1-S17** and **Table S1** are included.

AUTHOR INFORMATION

Corresponding Author

*E-mail: yksun@hanyang.ac.kr (Y. K. Sun).

*E-mail: husam.alshareef@kaust.edu.sa (H. Alshareef).

*E-mail: jun.ming@ciac.ac.cn (J. Ming).

Author Contributions

J. Ming, H. Alshareef and Y. Sun conceived the idea together. L. Zhou and W. Wahyudi carried out the electrochemical experiments. Z. Cao, L. Cavallo, and T. Anthopoulos carried out the simulations. J. Zhang, J. Hwang, Y. Cheng and L. Wang tested the Raman and NMR results. All authors analyzed the data and contributed to the discussion. L. Zhou, H. Alshareef, Y. Sun and J. Ming wrote the manuscript. † L. Zhou, Z. Cao and W. Wahyudi contributed equally.

ACKNOWLEDGEMENTS

This work is supported by the National Natural Science Foundation of China (21978281, 21975250) and National Key R&D Program of China (SQ2017YFE9128100). The authors also thank the Independent Research Project of the State Key Laboratory of Rare Earth Resources Utilization (110005R086), Changchun Institute of Applied Chemistry, Chinese Academy of Sciences. The research was also supported by King Abdullah University of Science and Technology (KAUST) and Hanyang University. The authors also acknowledege fruitful discussions with the research scientists at Huzhou Kunlun Power Battery Materials Co., LTD.

REFERENCES

1) Tarascon, J. M.; Armand, M., Issues and Challenges Facing Rechargeable Lithium Batteries. *Nature* **2001**, *414*, 359-367.

2) Hwang, J. Y.; Myung, S. T.; Sun, Y. K., Sodium-Ion Batteries: Present and Future. *Chem. Soc. Rev.* **2017**, *46*, 3529-3614.

3) Yu, C. Y.; Park, J. S.; Jung, H. G.; Chung, K. Y.; Aurbach, D.; Sun, Y. K.; Myung, S. T., $NaCrO_2$ Cathode for High-Rate Sodium-Ion Batteries. *Energy Environ. Sci.* **2015**, *8*, 2019-2026.

4) Ming, J.; Li, M.; Kumar, P.; Lu, A. Y.; Wahyudi, W.; Li, L. J., Redox Species-Based Electrolytes for Advanced Rechargeable Lithium Ion Batteries. *ACS Energy Lett.* **2016**, *1*, 529-534.

5) Liu, Z.; Yu, X. Y.; Lou, X. W.; Paik, U., Sb@C Coaxial Nanotubes as a Superior Long-Life and High-Rate Anode for Sodium Ion Batteries. *Energy Environ. Sci.* **2016**, *9*, 2314-2318.

6) Ming, J.; Li, M.; Kumar, P.; Li, L. J., Multilayer Approach for Advanced Hybrid Lithium Battery. *ACS Nano* **2016**, *10*, 6037-6044.

7) Wu, Y.; Wang, W.; Ming, J.; Li, M.; Xie, L.; He, X.; Wang, J.; Liang, S.; Wu, Y., An Exploration of New Energy Storage System: High Energy Density, High Safety, and Fast Charging Lithium Ion Battery. *Adv Funct. Mater.* **2019**, *29*, 1805978-1805984.

8) Zhang, W.; Liu, Y.; Guo, Z., Approaching High-Performance Potassium-Ion Batteries *via* Advanced Design Strategies and Engineering. *Sci Adv.* **2019**, *5*, eaav7412-eeav7424.

9) Jache, B.; Adelhelm, P., Use of Graphite as a Highly Reversible Electrode with Superior Cycle Life for Sodium-Ion Batteries by Making Use of Co-Intercalation Phenomena. *Angew. Chem. Int. Ed.* **2014**, *53*, 10169-10173.

10) Ming, J.; Cao, Z.; Wahyudi, W.; Li, M.; Kumar, P.; Wu, Y.; Hwang, J. Y.; Hedhili, M. N.; Cavallo, L.; Sun, Y. K.; Li, L. J., New Insights on Graphite Anode Stability in Rechargeable Batteries: Li Ion Coordination Structures Prevail over Solid Electrolyte Interphases. *ACS Energy Lett.* **2018**, *3*, 335-340.

11) Zhou, L.; Cheng, Y.; Sun, Q.; Sun, L.; Wang, L.; Wang, X.; Yin, D.; Wang, L.; Ming, J., High Alkaline Ions Storage Capacities of Hollow Interwoven Structured Sb/TiO_2 Particles: Galvanic Replacement Formation Mechanism and Volumetric Buffer Effect. *Chem. Commun.* **2018**, *54*, 4049-4052.

12) Zhang, L.; Wu, H. B.; Liu, B.; Lou, X. W., Formation of porous SnO_2 microboxes via selective leaching for highly reversible lithium storage. *Energy Environ. Sci.* **2014**, *7*, 1013-1017.

13) Li, W.; Li, H.; Lu, Z.; Gan, L.; Ke, L.; Zhai, T.; Zhou, H., Layered Phosphorus-like GeP5: A Promising Anode Candidate with High Initial Coulombic Efficiency and Large Capacity for Lithium Ion Batteries. *Energy Environ. Sci.* **2015**, *8*, 3629-3636.

14) Wang, C.; Wang, L.; Li, F.; Cheng, F.; Chen, J., Bulk Bismuth as a High-Capacity and Ultralong Cycle-Life Anode for Sodium-Ion Batteries by Coupling with Glyme-Based Electrolytes. *Adv. Mater.* **2017**, *29*, 1702212-1702218.

15) Lei, K.; Wang, C.; Liu, L.; Luo, Y.; Mu, C.; Li, F.; Chen, J., A Porous Network of Bismuth Used as the Anode Material for High-Energy-Density Potassium-Ion Batteries. *Angew Chem. Int. Ed.* **2018**, *57*, 4687-4691.

16) He, M.; Walter, M.; Kravchyk, K. V.; Erni, R.; Widmer, R.; Kovalenko, M. V., Monodisperse SnSb nanocrystals for Li-ion and Na-ion battery anodes: synergy and dissonance between Sn and Sb. *Nanoscale* **2015**, *7*, 455-459.

17) Zhu, Z.; Wang, S.; Du, J.; Jin, Q.; Zhang, T.; Cheng, F.; Chen, J., Ultrasmall Sn Nanoparticles Embedded in Nitrogen-Doped Porous Carbon As High-Performance Anode for Lithium-Ion Batteries. *Nano Lett.* **2014**, *14*, 153-157.

18) Pan, F.; Zhang, W.; Ma, J.; Yao, N.; Xu, L.; He, Y. S.; Yang, X.; Ma, Z. F., Integrating *in situ* Solvothermal Approach Synthesized Nanostructured Tin Anchored on Graphene Sheets into Film Anodes for Sodium-Ion Batteries. *Electrochim Acta* **2016**, *196*, 572-578.

19) Luo, W.; Calas, A.; Tang, C.; Li, F.; Zhou, L.; Mai, L., Ultralong Sb_2Se_3 Nanowire-Based Free-Standing Membrane Anode for Lithium/Sodium Ion Batteries. *ACS Appl. Mater. Intefaces* **2016**, *8*, 35219-35226.

20) Jiang, Y.; Wei, M.; Feng, J.; Ma, Y.; Xiong, S., Enhancing the Cycling Stability of Na-ion Batteries by Bonding SnS_2 Ultrafine Nanocrystals on Amino-Functionalized Graphene Hybrid Nanosheets. *Energy Environ. Sci.* **2016**, *9*, 1430-1438.

21) Sun, Q.; Wu, H.; Ming, H.; Sun, L.; Zhou, L.; Wang, C.; Wang, X.; Wang, L.; Ming, J., Bio-Inspired Self-Breathable Structure Driven by the Volumetric Effect: An Unusual Driving Force of Metal Sulfide for High Alkaline Ion Storage Capability. *J. Mater. Chem. A* **2019,** *7* (10), 5677-5684.

22) Huang, J.; Guo, X.; Du, X.; Lin, X.; Huang, J.; Tan, H.; Zhu, Y.; Zhang, B., Nanostructure of Solid Electrolyte Interphases and its Consequences For Microsized Sn Anodes in Sodium Ion Battery. *Energy Environ. Sci.* **2019**, *12*, 1550-1557.

23) Park, M. G.; Lee, D. H.; Jung, H.; Choi, J. H.; Park, C. M., Sn-Based Nanocomposite for Li-Ion Battery Anode with High Energy Density, Rate Capability, and Reversibility. *ACS Nano* **2018**, *12*, 2955-2967.

24) Zhang, B.; Rousse, G.; Foix, D.; Dugas, R.; Corte, D. A.; Tarascon, J. M., Microsized Sn as Advanced Anodes in Glyme-Based Electrolyte for Na-Ion Batteries. *Adv. Mater.* **2016**, *28*, 9824-9830.

25) Li, J.; Xu, H.; Li, S.; Zhang, C.; Long, C.; Jian, L.; Yong, X.; Zheng, Y.; Huang, Y., Roll-to-Roll Prelithiation of Sn Foil Anode Suppresses Gassing and Enables Stable Full-Cell Cycling of Lithium Ion Batteries. *Energy Environ. Sci.* **2019**, *12*, 2991-3000.

26) Suo, L.; Borodin, O.; Gao, T.; Olguin, M.; Ho, J.; Fan, X.; Luo, C.; Wang, C.; Xu, K., "Water-in-Salt" Electrolyte Enables High-Voltage Aqueous Lithium-Ion Chemistries. *Science* **2015**, *350,* 938-943.

27) Zheng, J.; Lochala, J. A.; Kwok, A.; Deng, Z. D.; Xiao, J., Research Progress towards Understanding the Unique Interfaces between Concentrated Electrolytes and Electrodes for Energy Storage Applications. *Adv. Sci.* **2017**, *4*, 1700032-1700050.

28) Lee, H.; Lim, H. S.; Ren, X.; Yu, L.; Engelhard, M. H.; Han, K. S.; Lee, J.; Kim, H. T.; Xiao, J.; Liu, J.; Xu, W.; Zhang, J. G., Detrimental Effects of Chemical Crossover from the Lithium Anode to Cathode in Rechargeable Lithium Metal Batteries. *ACS Energy Lett.* **2018**, *3*, 2921-2930.

29) Xiao, J., How Lithium Dendrites Form in Liquid Batteries. *Science* **2019**, *366,* 426-427.

30) Liu, J.; Bao, Z.; Cui, Y.; Dufek, E. J.; Goodenough, J. B.; Khalifah, P.; Li, Q.; Liaw, B. Y.; Liu, P.; Manthiram, A.; Meng, Y. S.; Subramanian, V. R.; Toney, M. F.; Viswanathan, V. V.; Whittingham, M. S.; Xiao, J.; Xu, W.; Yang, J.; Yang, X. Q.; Zhang, J. G., Pathways for Practical High-Energy Long-Cycling Lithium Metal Batteries. *Nat. Energy* **2019**, *4*, 180-186.

31) Fan, X.; Ji, X.; Chen, L.; Chen, J.; Deng, T.; Han, F.; Yue, J.; Piao, N.; Wang, R.; Zhou, X.; Xiao, X.; Chen, L.; Wang, C., All-Temperature Batteries Enabled by Fluorinated Electrolytes with Non-Polar Solvents. *Nat. Energy* **2019**, *4*, 882-890.

32) Qian, J.; Henderson, W. A.; Xu, W.; Bhattacharya, P.; Engelhard, M.; Borodin, O.; Zhang, J. G., High Rate and Stable Cycling of Lithium Metal Anode. *Nat. Commun.* **2015**, *6*, 6362.

33) Fan, X.; Chen, L.; Borodin, O.; Ji, X.; Chen, J.; Hou, S.; Deng, T.; Zheng, J.; Yang, C.; Liou, S. C.; Amine, K.; Xu, K.; Wang, C., Non-Flammable Electrolyte Enables Li-Metal Batteries with Aggressive Cathode Chemistries. *Nat. Nanotech.* **2018**, *13*, 715-722.

34) Niu, C.; Lee, H.; Chen, S.; Li, Q.; Du, J.; Xu, W.; Zhang, J. G.; Whittingham, M. S.; Xiao, J.; Liu, J., High-Energy Lithium Metal Pouch Cells with Limited Anode Swelling and Long Stable Cycles. *Nat. Energy* **2019**, *4*, 551-559.

35) Niu, C.; Pan, H.; Xu, W.; Xiao, J.; Zhang, J. G.; Luo, L.; Wang, C.; Mei, D.; Meng, J.; Wang, X.; Liu, Z.; Mai, L.; Liu, J., Self-Smoothing Anode for Achieving High-Energy Lithium Metal Batteries under Realistic Conditions. *Nat. Nanotech.* **2019**, *14*, 594-601.

36) Cao, X.; Ren, X.; Zou, L.; Engelhard, M. H.; Huang, W.; Wang, H.; Matthews, B. E.; Lee, H.; Niu, C.; Arey, B. W.; Cui, Y.; Wang, C.; Xiao, J.; Liu, J.; Xu, W.; Zhang, J. G., Monolithic Solid-Electrolyte Interphases Formed in Fluorinated Orthoformate-based Electrolytes Minimize Li Depletion and Pulverization. *Nat. Energy* **2019**, *4*, 796-805.

37) Zhang, H.; Huang, X.; Noonan, O.; Zhou, L.; Yu, C., Tailored Yolk–Shell Sn@C Nanoboxes for High-Performance Lithium Storage. *Adv Funct Mater* **2017**, *27*, 1606023-1606028.

38) Zhu, H.; Jia, Z.; Chen, Y.; Weadock, N.; Wan, J.; Vaaland, O.; Han, X.; Li, T.; Hu, L., Tin Anode for Sodium-Ion Batteries Using Natural Wood Fiber as a Mechanical Buffer and Electrolyte Reservoir. *Nano Lett.* **2013**, *13*, 3093-3100.

39) Hoar, T. P.; Jacob, W. R., Breakdown of Passivity of Stainless Steel by Halide Ions. *Nature* **1967**, *216*, 1299-1301.

40) Sun, M. Z.; Shi, S. Q.; Huang, B. L., Blue Energy Case Study and Analysis: Attack of Chloride Ions on Chromia Passive Film on Metallic Electrode Of Nanogenerator. *Nano Energy* **2019**, *62*, 103-110.

41) Wang, C.; Meng, Y. S.; Xu, K., Perspective-Fluorinating Interphases. *J. Electrochem. Soc.* **2018**, *166*, A5184-A5186.

42) Wu, B.; Wang, S.; Lochala, J.; Desrochers, D.; Liu, B.; Zhang, W.; Yang, J.; Xiao, J., The Role of the Solid Electrolyte Interphase Layer in Preventing Li Dendrite Growth in Solid-State Batteries. *Energy Environ. Sci.* **2018**, *11*, 1803-1810.

43) Wang, L.; Menakath, A.; Han, F.; Wang, Y.; Zavalij, P. Y.; Gaskell, K. J.; Borodin, O.; Iuga, D.; Brown, S. P.; Wang, C.; Xu, K.; Eichhorn, B. W., Identifying the Components of the Solid-Electrolyte Interphase in Li-Ion Batteries. *Nat. Chem.* **2019**, *11*, 789-796.

44) Lochala, J.; Taverne, T.; Wu, B.; Benamara, M.; Cai, M.; Xiao, X.; Xiao, J., Tuning Solid Electrolyte Interphase Layer Properties through the Integration of Conversion Reaction. *ACS Appl. Mater. Interfaces* **2019**, *11*, 44204-44213.

45) Ming, J.; Cao, Z.; Li, Q.; Wahyudi, W.; Wang, W.; Cavallo, L.; Park, K. J.; Sun, Y. K.; Alshareef, H. N., Molecular-Scale Interfacial Model for Predicting Electrode Performance in Rechargeable Batteries. *ACS Energy Lett.* **2019**, *4*, 1584-1593.

46) Logan, E. R.; Tonita, E. M.; Gering, K. L.; Li, J.; Ma, X.; Beaulieu, L. Y.; Dahn, J. R., A Study of the Physical Properties of Li-Ion Battery Electrolytes Containing Esters. *J. Electrochem. Soc.* **2018**, *165*, A21-A30.

47) Ponrouch, A.; Marchante, E.; Courty, M.; Tarascon, J. M.; Palacín, M. R., In Search of an Optimized Electrolyte for Na-Ion Batteries. *Energy Environ. Sci.* **2012**, *5*, 8572-8583.

48) Xuan, X.; Wang, J.; Wang, H., Theoretical insights into PF_6^- and its Alkali Metal Ion Pairs: Geometries and Vibrational Frequencies. *Electrochim Acta* **2005**, *50*, 4196-4201.

49) Xiao, N.; McCulloch, W. D.; Wu, Y., Reversible Dendrite-Free Potassium Plating and Stripping Electrochemistry for Potassium Secondary Batteries. *J. Am. Chem. Soc.* **2017**, *139* (28), 9475-9478.

50) Poater, A.; Cosenza, B.; Correa, A.; Giudice, S.; Ragone, F.; Scarano, V.; Cavallo, L., SambVca: A Web Application for the Calculation of the Buried Volume of N-Heterocyclic Carbene Ligands. *Eur. J. Inor. Chem.* **2009**, *13*, 1759-1766.

51) Wahyudi, W.; Cao, Z.; Kumar, P.; Li, M.; Wu, Y.; Hedhili, M. N.; Anthopoulos, T. D.; Cavallo, L.; Li, L. J.; Ming, J., Phase Inversion Strategy to Flexible Freestanding Electrode: Critical Coupling of Binders and Electrolytes for High Performance Li-S Battery. *Adv. Funct. Mater.* **2018**, *28*, 1802244-1802251.

52) Rajput, N. N.; Murugesan, V.; Shin, Y.; Han, K. S.; Lau, K. C.; Chen, J.; Liu, J.; Curtiss, L. A.; Mueller, K. T.; Persson, K. A., Elucidating the Solvation Structure and Dynamics of Lithium Polysulfides Resulting from Competitive Salt and Solvent Interactions. *Chem Mater.* **2017**, *29*, 3375-3379.

53) Wang, W.; Cao, Z.; Elia, G. A.; Wu, Y.; Wahyudi, W.; Abou-Hamad, E.; Emwas, A. H.; Cavallo, L.; Li, L. J.; Ming, J., Recognizing the Mechanism of Sulfurized Polyacrylonitrile

Cathode Materials for Li–S Batteries and beyond in Al–S Batteries. *ACS Energy Lett.* **2018**, *3*, 2899-2907.

54) Xu, K.; Zhang, S. S.; Jow, T. R., Formation of the Graphite/Electrolyte Interface by Lithium Bis(oxalato)borate. *Electrochem Solid State Lett.* **2003**, *6,* A117-A120.

55) Xu, K., Nonaqueous Liquid Electrolytes for Lithium-based Rechargeable Batteries. *Chem. Rev.* **2004**, *104*, 4303-4417.

56) Xu, K.; Zhang, S. S.; Jow, T. R., LiBOB as Additive in $LiPF_6$-Based Lithium Ion Electrolytes *Electrochem Solid State Lett.* **2005**, *7*, A365-A368.

57) Xu, K., Electrolytes and Interphases in Li-Ion Batteries and Beyond. *Chem. Rev.* **2014**, *114*, 11503-11618.

58) Xing, L. D.; Zheng, X. W.; Schroeder, M.; Alvarado, J.; Cresce, A. V.; Xu, K.; Li, Q. S.; Li, W. S., Deciphering the Ethylene Carbonate-Propylene Carbonate Mystery in Li-Ion Batteries. *Acc. Chem. Res.* **2018**, *51*, 282-289.

59) Von Wald Cresce, A.; Gobet, M.; Borodin, O.; Peng, J.; Russell, S. M.; Wikner, E.; Fu, A.; Hu, L.; Lee, H. S.; Zhang, Z.; Yang, X. Q.; Greenbaum, S.; Amine, K.; Xu, K., Anion Solvation in Carbonate-Based Electrolytes. *J. Phy. Chem. C* **2015**, *119*, 27255-27264.

60) Xu, K.; Lam, Y.; Zhang, S. S.; Jow, T. R.; Curtis, T. B., Solvation Sheath of Li^+ in Nonaqueous Electrolytes and Its Implication of Graphite/Electrolyte Interface Chemistry. *J. Phys. Chem. C* **2007**, *111,* 7411-742.

61) Lu, D. P.; Tao, J. H.; Yan, P. F.; Henderson, W. A.; Li, Q. Y.; Shao, Y. Y.; Helm, M. L.; Borodin, O.; Graff, G. L.; Polzin, B.; Wang, C. M.; Engelhard, M.; Zhang, J. G.; De Yoreo, J. J.; Liu, J.; Xiao, J., Formation of Reversible Solid Electrolyte Interface on Graphite Surface from Concentrated Electrolytes. *Nano Lett.* **2017**, *17*, 1602-1609.